ACS APPLIED MATERIALS & INTERFACES

Research Article

www.acsami.org

Highly Enhanced Sensing Properties for ZnO Nanoparticle-Decorated Round-Edged α-Fe_2O_3 Hexahedrons

Xin Zhou, Yan Xiao, Meng Wang, Peng Sun,* Fengmin Liu, Xishuang Liang, Xiaowei Li, and Geyu Lu*

State Key Laboratory on Integrated Optoelectronics, College of Electronic Science and Engineering, Jilin University, Changchun 130012, People's Republic of China

Supporting Information

ABSTRACT: ZnO/α-Fe_2O_3 composites built from plenty of ZnO nanoparticles decorated on the surfaces of uniform round-edged α-Fe_2O_3 hexahedrons were successfully prepared via a facile solvothermal method. Various techniques were employed to obtain the crystalline and morphological characterization of the as-prepared samples. In addition, a comparative sensing performance investigation between the two kinds of sensing materials clearly demonstrated that the sensing properties of ZnO/α-Fe_2O_3 composites were substantially enhanced compared with those of the single α-Fe_2O_3 component, which manifest the superiority of the ZnO decoration as we expected. For instance, the response of ZnO/α-Fe_2O_3 composites to 100 ppm acetone is ~30, which is ~3.15-fold higher than that of primary α-Fe_2O_3 hexahedrons. The synergetic effect is believed to be the source of the improvement of gas-sensing properties.

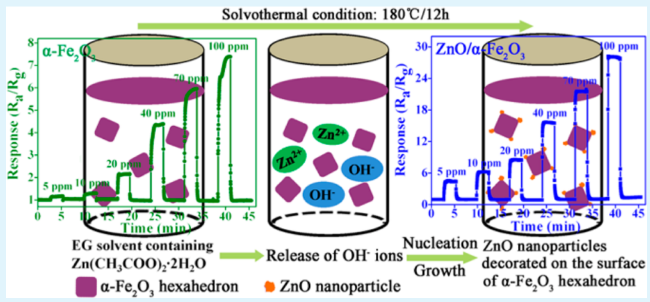

KEYWORDS: *α-Fe_2O_3 hexahedron, ZnO/α-Fe_2O_3 composites, solvothermal method, semiconductor, gas sensor*

1. INTRODUCTION

In light of the fascinating merits of easy manufacture, low cost and power consumption, as well as wide detection range, gas sensors based on oxide semiconductors stand out from numerous detection methods and have been regarded as a dominant and effective approach in the monitoring of various flammable, toxic, and corrosive gases.[1] Until now, various kinds of metal oxides, such as ZnO,[2,3] α-Fe_2O_3,[4,5] WO_3,[6,7] In_2O_3,[8,9] SnO_2,[10,11] NiO,[12] etc., have been extensively investigated as sensing materials owing to their superior stability, low cost, and simplicity in preparation.[13,14] It has been widely acknowledged that the basic working principle of metal oxide-based gas sensors is the remarkable resistance change caused by the surface reaction upon exposure to different gas ambients. Therefore, in terms of metal oxide semiconductors, the chemical composition, crystalline size, and microstructure have essential impact on their sensing properties.[12] On the basis of this consensus, considerable efforts, including transition metal doping, novel metal loading, as well as the compounds consisting of chemically distinct components, have been devoted to improve gas-sensing performance.[15] Among these strategies, composites constituted by two or more metal oxides such as α-Fe_2O_3/SnO_2,[16,17] ZnO/SnO_2,[18,19] SnO_2/α-Fe_2O_3,[20,21] have drawn increasing attention as they are supposed to provide more opportunities for integrating the physical and chemical properties of their individual counterparts, and this method indeed enhanced the sensing performances.[22] However, in spite of the significant accomplishments achieved, developing new sensor strategies for ever-increasing response, fast detection, good reproducibility, and reduction of cost still represents one of the major scientific challenges owing to the constant growing concerns about air-quality, environmental monitoring, and explosive gases detection. Therefore, the synthesis of new-type composites to achieve dramatic improvement in gas-sensing properties deserves more efforts.

Two kinds of important functional materials, namely, hematite (α-Fe_2O_3) and zinc oxide (ZnO), with energy gaps of ~2.2 eV[23] and ~3.4 eV,[24] respectively, have been widely investigated in a broad range of applications involving gas sensors,[25,26] photocatalysis,[27,28] magnetic materials,[29,30] lithium-ion batteries,[31,32] and solar cells.[33,34] Recent researches have demonstrated that the gas-sensing performances of α-Fe_2O_3 could be greatly improved by the modification of ZnO nanoparticles, which can be attributed to the synergistic effect of the two sensing components. However, to the best of our knowledge, despite some success having been achieved for the preparation of ZnO/α-Fe_2O_3 composites, there still exist some disadvantages, such as the high temperature involved in the synthesis process (>350 °C) or the complete enclosure of the α-Fe_2O_3 core by the ZnO shell, which reduced the adsorption of oxygen molecules on the surface of the α-Fe_2O_3, leading to the sensing performances not improved but reduced.[35,36] Therefore, developing a facile and effective strategy under moderate conditions for the preparation of ZnO/α-Fe_2O_3

Received: February 4, 2015
Accepted: April 13, 2015
Published: April 13, 2015

ACS Publications © 2015 American Chemical Society

composites with highly accessible surfaces that benefits the gas adsorption is quite important.

In the current work, the novel and uniform α-Fe_2O_3 hexahedrons made up of numerous nanoparticles were first synthesized through a facile solvothermal route. Although the as-prepared α-Fe_2O_3 showed high response to acetone, to further enhance their gas sensing properties, ZnO nanoparticles were decorated on the surfaces of α-Fe_2O_3 hexahedrons to form ZnO/α-Fe_2O_3 composites. As expected, it is clearly revealed that ZnO/α-Fe_2O_3 composites showed much higher response along with faster response rate to acetone than that of the pristine α-Fe_2O_3. The dramatic improvement in gas-sensing properties may be ascribed to the synergistic effect exerted by ZnO and α-Fe_2O_3 and the introduction of ZnO layer with particle size comparable to the Deybe length.

2. EXPERIMENTAL SECTION

All of the chemical reagents involved in the experiment were analytical grade as purchased from Beijing Chemicals Co. Ltd. of China and directly used without any further purification.

2.1. Synthesis of Round-Edged α-Fe_2O_3 Hexahedrons. Round-edged α-Fe_2O_3 hexahedrons were successfully synthesized through a simple solvothermal method according to the previous literature with some modifications.[37] Generally, 4.054 g of iron chloride hexahydrate ($FeCl_3{\cdot}6H_2O$) was dissolved into a mixture solution of 15 mL of ethanol and 15 mL of deionized water under vigorously magnetic stirring. Subsequently, 1.2 g of hexamethylenetetramine ($(CH_2)_6N_4$, HMT) was added into the above solution. After several minutes of ultrasonic dispersing, the homogeneous solution was transferred into a Teflon-lined stainless steel autoclave, which was then tightly sealed and maintained at 160 °C for 6 h in an electric oven. Then, the autoclave was cooled naturally to room temperature, and the resultant precipitates were harvested by centrifugation, rinsed several times with ethanol and deionized water, and finally dried at 80 °C for 12 h.

2.2. Synthesis of ZnO/α-Fe_2O_3 Composites. In a typical procedure, 0.055 g of $Zn(CH_3COO)_2{\cdot}2H_2O$ was first dissolved in 10 mL of ethylene glycol (EG) until a clear solution was achieved. Then, 0.040 g of the presynthesized α-Fe_2O_3 hexahedron was well-sonicated into the above solution and stirred for 30 min. Soon after, the solution was transferred to a Teflon-lined stainless steel autoclave, which was sealed, kept at 180 °C for 12 h, and then cooled to room temperature naturally. The products were collected by centrifugation and washed with deionized water and ethanol several times and finally dried at 80 °C for 12 h.

2.3. Characterization. X-ray powder diffraction (XRD) analysis was performed on a Rigaku D/Max-2550 V X-ray diffractometer with high-intensity Cu Kα radiation (λ = 1.5406 Å) in the range of 20——70° (2θ) to examine the crystal phase and purity of the as-obtained samples. The morphology and size of the products were studied by field emission scanning electron microscopy (FESEM, JEOL JSM-7500F, operated at an accelerating voltage of 15 kV).Transmission electron microscopy (TEM) and high-resolution transmission electron microscopy (HRTEM) observations were carried out with JEOL JEM-2100 microscope operated at an accelerating voltage of 200 kV. The energy-dispersive X-ray spectrometry (EDS) was applied to study the chemical compositions of the products, which was measured by the TEM attachment.

2.4. Fabrication and Measurement of Gas Sensor. The sensor fabrication process was described detailedly in our previous work,[38] and the gas-sensing behavior was estimated by an RQ-2 gas-sensing characterization system under laboratory conditions (40% relative humidity, 23 °C). The specific measurement was processed by a static process: the sensor was placed into a chamber filled with fresh air at the beginning, and then an appropriate amount of the test gas was injected into a closed chamber by the assistance of a microsyringe. Soon afterward, the sensor was put into the chamber to react with the test gas molecules. After a constant response value obtained, the sensor was transferred into another chamber also full of fresh air and began to recover. The gas response S ($S = R_a/R_g$) was defined as the ratio of sensor resistance in fresh air (R_a) to that in test gases (R_g). The time taken by the sensor to achieve 90% of the total resistance change in the case of adsorption and desorption was defined as the response time (τ_{res}) and recovery time (τ_{recov}), respectively.

3. RESULTS AND DISCUSSION

3.1. Structural and Morphological Characteristics. XRD analysis associated with pure α-Fe_2O_3 and ZnO/α-Fe_2O_3 composites was performed to investigate the crystal structure and purity of the samples, which is depicted in Figure 1. The XRD pattern (Figure 1a) of the bare α-Fe_2O_3

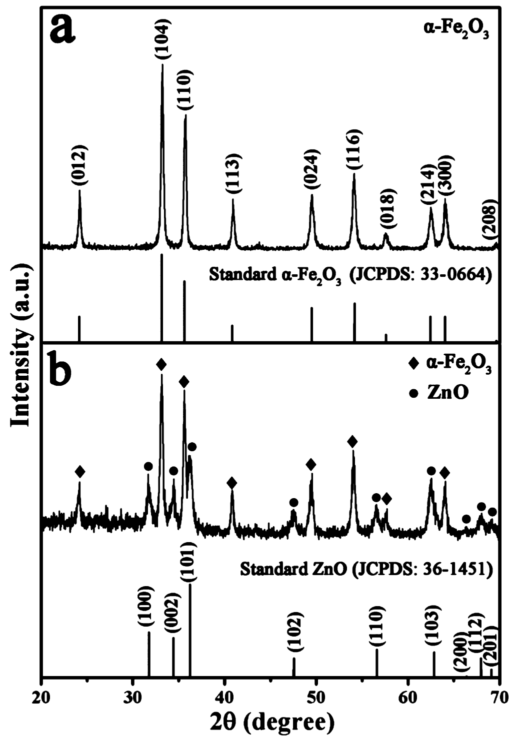

Figure 1. XRD patterns of the as-obtained products (a) round-edged α-Fe_2O_3 hexahedrons and (b) ZnO/α-Fe_2O_3 composites.

hexahedrons exhibited very sharp diffraction peaks, indicating their high crystallinity, and all of the recorded diffraction peaks could be well-assigned to the pure hexagonal structure of α-Fe_2O_3 with lattice constants of $a = b$ = 5.04 Å and c = 13.77 Å, which is in good accordance with those from the standard JCPDS Card No. 33−0664. Meanwhile, XRD pattern of composites shown in Figure 1b clearly revealed that the crystal phases are the mixture of α-Fe_2O_3 and ZnO; most of the identified diffraction peaks could be unambiguously assigned to the hexagonal structure of α-Fe_2O_3. The residual peaks could be readily indexed to the hexagonal structure of ZnO with structural parameters of $a = b$ = 3.25 Å and c = 5.21 Å, which is in good accordance with the standard data file No. 36−1451. Notably, it also shown that the ZnO decoration process does not deteriorate the original crystal structure of hematite since all diffraction peaks for hematite phase in the ZnO/α-Fe_2O_3 composites exist at almost the same 2θ position as that for the as-obtained α-Fe_2O_3 hexahedrons, and no diffraction peaks derived from any other impurities could be observed, demonstrating the high purity of the samples.

DOI: 10.1021/acsami.5b01071
ACS Appl. Mater. Interfaces 2015, 7, 8743−8749

The size and morphology of pristine α-Fe_2O_3 and ZnO-modified α-Fe_2O_3 were investigated by FESEM, as exhibited in Figure 2. The representative low-magnification FESEM image

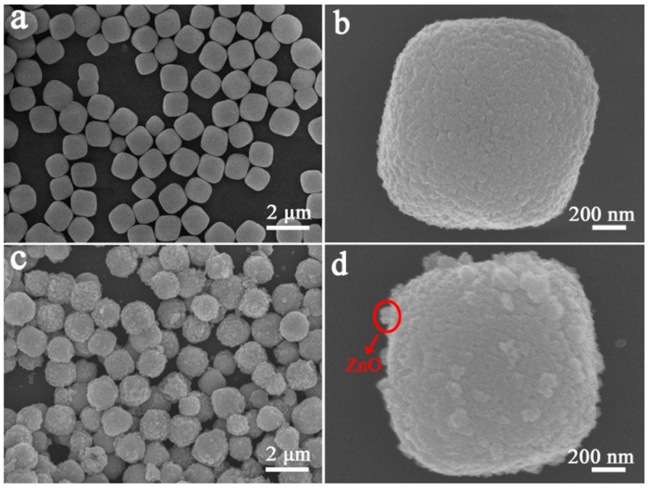

Figure 2. FESEM images of the as-prepared products, (a) and (b) pristine α-Fe_2O_3 hexahedrons, (c) and (d) ZnO/α-Fe_2O_3 composites.

(presented in Figure 2a) of the as-obtained α-Fe_2O_3 hexahedrons clearly revealed that the sample has a good dispersivity and a uniform size of ~1.2 μm. No other morphologies could be observed, indicating the high yield of the products. Moreover, it can be clearly observed that the as-prepared α-Fe_2O_3 samples have a relatively smooth surface from the high-magnification FESEM image of an individual α-Fe_2O_3 hexahedron presented in Figure 2b. The typical FESEM image of resulting products (shown in Figure 2c) undoubtedly revealed that the surfaces of the ZnO/α-Fe_2O_3 composites turn coarser compared with the pristine α-Fe_2O_3 hexahedrons, which can be assigned to the successful decoration of the secondary ZnO nanoparticles on the pristine α-Fe_2O_3 substrates. In addition, the FESEM image of a single ZnO-modified α-Fe_2O_3 hexahedron (exhibited in Figure 2d) further verified that massive ZnO nanoparticles were coated on the surfaces of α-Fe_2O_3 hexahedron and that the morphology of α-Fe_2O_3 was perfectly maintained, instead of destroyed, when compared with the FESEM images of pure α-Fe_2O_3 presented in Figure 2a,b. And, these rough surfaces are deduced to be favorable for gas detection, owing to the rapid and effective gas diffusion between the inward and outward; therefore, good gas-sensing performances could be anticipated.[39]

TEM measurements were also performed to provide insight into more-detailed structural and crystalline information on the as-prepared ZnO/α-Fe_2O_3 composites. Representative TEM images presented in Figure 3a,b explicitly manifest that the samples are constructed by round-edged α-Fe_2O_3 hexahedrons, which are solid in nature and are not completely enclosed by ZnO nanoparticles. And, both morphology and size of bare α-Fe_2O_3 and ZnO nanoparticle observed from TEM observations are in good accordance with the FESEM measurement results. HRTEM image provides further insight into the crystal structure of ZnO nanoparticles, which was exhibited in Figure 3c (recorded from the bottom section marked with a red rectangle in Figure 3b). The magnified HRTEM images in Figure 3d,e present clear lattice fringes with interplanar lattice spacings of 0.19 and 0.26 nm, corresponding to the (102) and (002) planes of hexagonal ZnO structure, respectively. EDS elemental mapping analysis corresponding to an individual ZnO/α-Fe_2O_3 hexahedron (Figure 3f) distinctly reveals spatial distributions of Fe, Zn, and O elements (Figure 3g−i). It is worth noting that the Fe signals could only be detected in the core region, while Zn signals were predominant in the outer region, and the uneven distribution of Zn element further confirmed that the surface of α-Fe_2O_3 hexahedron was not completely enclosed by ZnO nanoparticles; O signals can be recognized from the inside to outside of the range.

3.2. Gas-Sensing Performances. In the gas-sensing study, it is known to all that the operating temperature plays an essential role in determining the gas-sensing properties owing to its huge impact on surface state of sensing materials, as well as the interaction between the absorbed oxygen and sensing materials.[40] Therefore, the relationships between the operating temperatures and gas responses to 100 ppm acetone of the two kinds of sensor devices were first investigated in the temperature range of 200−350 °C, which are shown in Figure 4a. Since the test gas molecules are not active enough to

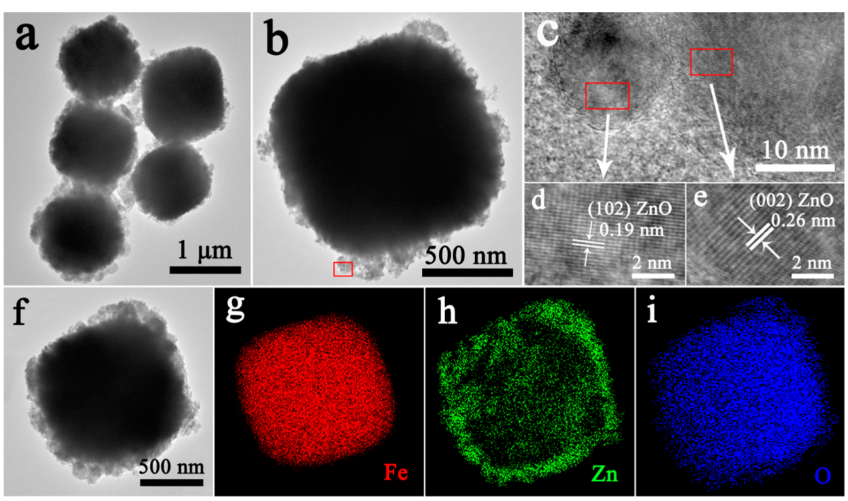

Figure 3. (a, b) Typical TEM images of the as-prepared ZnO/α-Fe_2O_3 composites. (c) HRTEM image of the marked section in (b). (d, e) Magnified HRTEM images recorded in different areas of (c). (f−i) TEM image of an individual ZnO/α-Fe_2O_3 hexahedron and the corresponding elemental mapping images.

DOI: 10.1021/acsami.5b01071
ACS Appl. Mater. Interfaces 2015, 7, 8743−8749

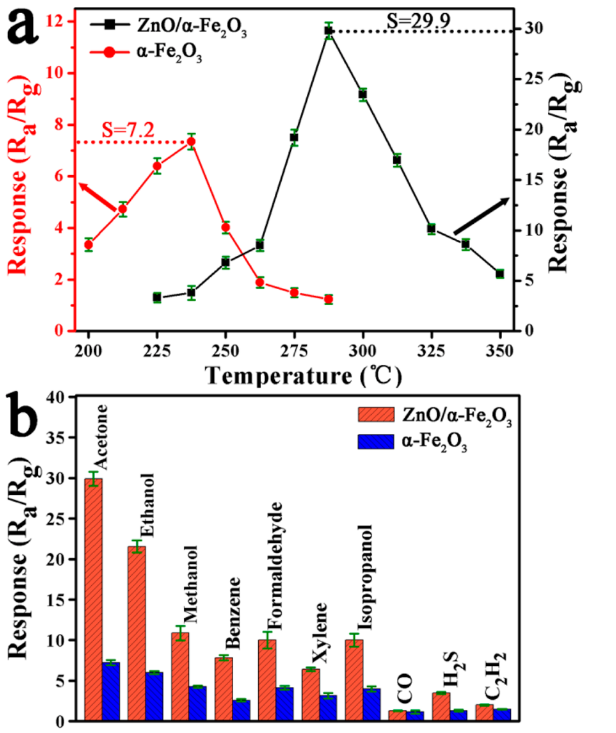

Figure 4. (a) Responses of pure α-Fe_2O_3 and ZnO/α-Fe_2O_3 composites upon exposure to 100 ppm acetone at different operating temperatures. (b) Selectivity measurements of the pristine α-Fe_2O_3 and ZnO/α-Fe_2O_3 composites to various test gases with concentrations of 100 ppm. The error bars denote the standard errors of the mean values of three independent measurements.

overcome the activation energy barrier to react with the surface-absorbed oxygen species at a low temperature, while at temperatures that are too high the difficulty in gas adsorption in turn causes the low utilization rate of the sensing material; thus, low gas responses were achieved in both of the two situations.[41−43] Hence, an "increase−maximum−decay" tendency was obtained along with the temperature increasing. More noticeable, for pure α-Fe_2O_3, the maximum response is 7.2 at 240 °C, while in the ZnO/α-Fe_2O_3 composite case, the maximum response of 29.9 appears at 290 °C, which is as 4.15-fold high as bare α-Fe_2O_3 hexahedrons. Accordingly, 240 and 290 °C were selected as the optimum operating temperatures for the two gas sensors and applied in all investigations hereinafter.

Since selectivity is a remarkable aspect of sensing properties, α-Fe_2O_3 hexahedrons and ZnO/α-Fe_2O_3 composites-based gas sensors of various kinds of test gases (such as acetone, ethanol, methanol, formaldehyde, and so on) with concentrations of 100 ppm were investigated at 240 and 290 °C, respectively (shown in Figure 4b). Obviously, both of the sensor devices exhibited much higher response to acetone as opposed to other test gases, indicating the good selectivity for acetone. In addition, it is worth noting that the gas responses were all improved after the ZnO nanoparticle decoration, and the largest increase can be observed for acetone, which is as 4.15-fold as high as the pristine α-Fe_2O_3. Therefore, it is concluded that after the modification of ZnO nanoparticles, a remarkable enhancement and excellent selectivity in acetone-sensing properties were obtained for ZnO/α-Fe_2O_3 composites.

Figure 5 exhibits the response behaviors of sensors to different concentrations of acetone at the optimum operating temperatures. Apparently, the gas responses of the two sensors both present a stepwise distribution accompanied by the increasing of acetone concentration, and the acetone-sensing properties were significantly improved for ZnO/α-Fe_2O_3 composites when compared with that of pure α-Fe_2O_3. Figure 5b depicts the temporal response and recovery curves for the two types of sensor devices, which were measured by orderly exposing the sensors to acetone with the concentration range from 5 to 100 ppm at 240 and 290 °C, respectively. The corresponding response values of ZnO/α-Fe_2O_3 composites were ~4.7, 6.5, 8.9, 14.9, 16.9, 20.5, 21.6, 23, 25.9, 27.2, and

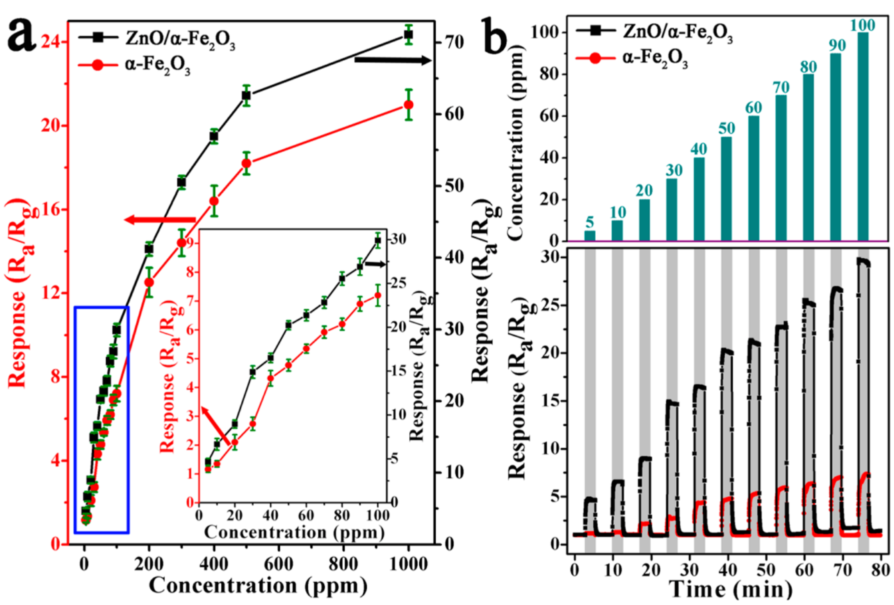

Figure 5. (a) Responses vs acetone concentration for ZnO/α-Fe_2O_3 composites at 290 °C and pure α-Fe_2O_3 at 240 °C. (b) Dynamic response curves of pristine α-Fe_2O_3 and ZnO/α-Fe_2O_3 composites to different concentrations of acetone. The error bars denote the standard errors of the mean values of three independent measurements.

DOI: 10.1021/acsami.5b01071
ACS Appl. Mater. Interfaces 2015, 7, 8743−8749

29.9, while for the primary α-Fe_2O_3 case, the response values were merely 1.1, 1.4, 2.1, 2.4, 2.9, 4.4, 4.8, 5.4, 6.2, 6.9, and 7.2. Accordingly, it can be unambiguously concluded that the modification of secondary ZnO nanoparticles could make the acetone-sensing performances substantially enhanced.

From the perspective of practical application of sensor device, not only high response but also fast response speed should be paid attention to, on account of their vital roles in avoiding possible loss and disasters. The dynamic response curve shown in Figure 6a explicitly demonstrated the ZnO/α-Fe_2O_3 composites exhibit excellent response and recovery characteristics toward 20 ppm acetone, ethanol, and methanol. In addition, it can be apparently observed that the response time (τ_{res}) of ZnO/α-Fe_2O_3 composites to 20 ppm acetone was as low as 1 s, which was far less than that of ethanol (3 s) and methanol (9 s) (Figure 6b). The recovery times (τ_{recov}) were within 35, 36, and 32 s for acetone, ethanol, and methanol, respectively (Figure 6b). Furthermore, the response features of ZnO/α-Fe_2O_3 composites-based sensor were well-repeated, and there is no clear floating in responses during the five reversible cycle measurement to 20 ppm acetone, indicating the excellent reproducibility of the gas sensor (Figure S1 of the Supporting Information).

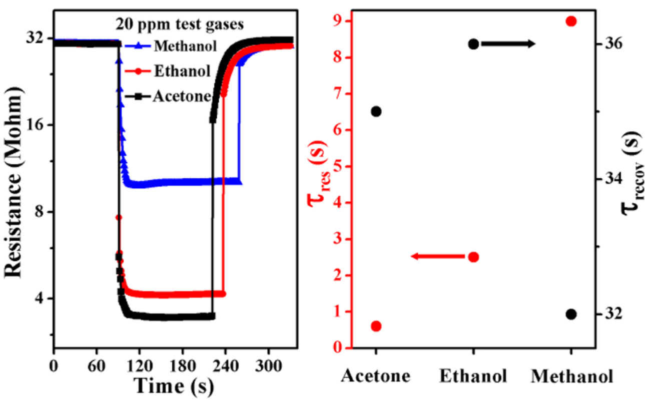

Figure 6. (a) Response transients of ZnO/α-Fe_2O_3 composites to acetone, ethanol, and methanol with a concentration of 20 ppm at 290 °C. (b)The corresponding response times and recovery times.

3.3. Formation Mechanism of ZnO/α-Fe_2O_3 Composites.

The plausible growth mechanism for ZnO nanoparticles in the second-step solvothermal process was discussed and described in the following. First of all, the etherification reaction[44,45] between EG molecules took place, leading to the release of a large quantity of water molecules, which are necessary for the subsequent hydrolysis of Zn^{2+}. Afterward, with a rising of temperature, OH^- ions were produced by the hydrolysis of CH_3COO^- ions, resulting in a base condition obtained:[46]

$$CH_3COO^- + H_2O \rightarrow CH_3COOH + OH^- \quad (1)$$

Soon after, Zn^{2+} ions react with OH^- ions generated by the hydrolysis of CH_3COO^- to form zinc hydroxide ($Zn(OH)_2$).[22]

$$Zn^{2+} + 2OH^- \rightarrow Zn(OH)_2 \quad (2)$$

The formation of ZnO was attributed to the decomposition of $Zn(OH)_2$ under high-temperature solvothermal reaction:

$$Zn(OH)_2 \rightarrow ZnO + H_2O \quad (3)$$

3.4. Gas-Sensing Mechanism.

As typical n-type semiconductor oxides, the most widely accepted gas-sensing mechanism for ZnO and α-Fe_2O_3 should follow the space charge model, which may be explained by the change in resistance of the sensor upon exposed to different gas atmospheres.[47,48] In ambient air, sensing materials can absorb oxygen molecules (O_2) and form surface-adsorbed oxygen species ($O^-_{2(ads)}$, $O^-_{(ads)}$, and $O^{2-}_{(ads)}$, eqs 4−7) by capturing free electrons from their conduction bands. The reaction kinematics can be described as follows:[49]

$$O_2 \rightarrow O_{2(ads)} \quad (4)$$

$$O_{2(ads)} + e^- \rightarrow O_2{}^-{}_{(ads)} \quad (5)$$

$$O_2{}^-{}_{(ads)} + e^- \rightarrow 2O^-_{(ads)} \quad (6)$$

$$O^-_{(ads)} + e^- \rightarrow O^{2-}_{(ads)} \quad (7)$$

In this process, a thick electron depletion layer formed on the surface area, resulting in a decrease of carrier concentration and increase of sensor resistance in coincidence (Figure 7a). When the sensor is exposed to reducing gases, for instance, acetone and ethanol at a moderate temperature, the adsorbed oxygen species will take part in the reaction with these gas molecules to form CO_2 and H_2O (eqs 8−10).The reactions between reducing gases and the surface adsorbed oxygen species can be described as follows:[34,50]

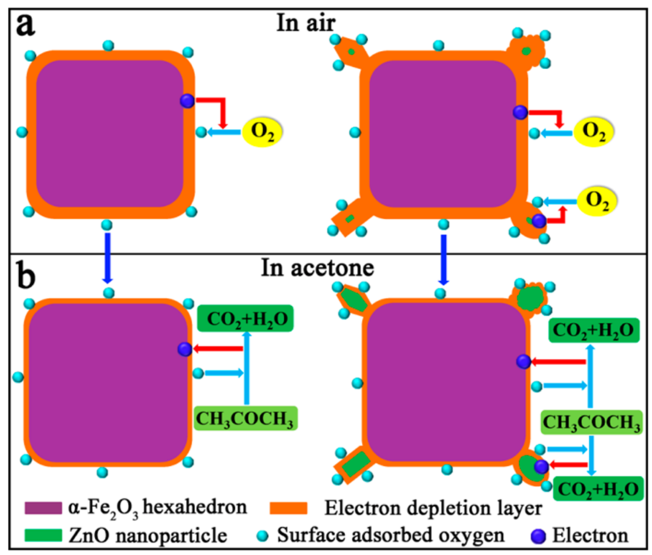

Figure 7. (a, b) Schematic illustration of sensing mechanism of α-Fe_2O_3 hexahedron, ZnO/α-Fe_2O_3 composite, and the possible reason for ZnO/α-Fe_2O_3 composites with higher gas response to acetone.

$$C_3H_6O + 8O^-_{(ads)} \rightarrow 3CO_2 + 3H_2O + 8e^- \quad (8)$$

$$C_2H_5OH + 6O^-_{(ads)} \rightarrow 2CO_2 + 3H_2O + 6e^- \quad (9)$$

$$CH_3OH + 3O^-_{(ads)} \rightarrow CO_2 + 2H_2O + 3e^- \quad (10)$$

As a consequence, the electrons trapped in the ionized oxygen species were released back into the conduction band, leading to the thickness of electron depletion layer decreases and lowering the measured resistance of the sensor (Figure 7b).

It has been clearly revealed that the ZnO nanoparticle-decorated α-Fe_2O_3 nanostructure exhibited much better

DOI: 10.1021/acsami.5b01071
ACS Appl. Mater. Interfaces 2015, 7, 8743−8749

sensing performances than that of the pristine one, indicating ZnO nanoparticle modification contributed greatly to the improvement of sensing properties. The dramatic enhancement in sensing properties of ZnO/α-Fe_2O_3 composites can be attributed to the following two factors. First, the striking synergistic effect of the two metal oxides.[51] For the as-prepared ZnO-modified α-Fe_2O_3 hexahedron, the surfaces of α-Fe_2O_3 hexahedron are not completely enclosed by ZnO nanoparticles, resulting in both of them being highly accessible for the adsorption of oxygen molecules and promoting the formation of depletion layers on the surfaces of both metal oxides while exposed to air. Therefore, both α-Fe_2O_3 and ZnO contribute to acetone response (Figure 7b). Second, it has been revealed that the gas response would obtain an abrupt increase when the particle size becomes comparable to or smaller than the Debye length.[52,53] In our case, the average size of ZnO nanoparticles is ~15−20 nm according to the TEM measurement results (Figure 3), which is comparable to the Debye length of ZnO (in the temperature range of 100−400 °C, the Debye length of ZnO is evaluated to be ~20 ± 5 nm),[54] leading to the electrons in ZnO being almost completely depleted, and this has a positive effect on gas response (Figure 7a).

4. CONCLUSIONS

In summary, a facile and controllable solution route was employed for the preparation of uniform ZnO/α-Fe_2O_3 composites, which were constructed by large numbers of ZnO nanoparticles decorated on the surfaces of round-edged α-Fe_2O_3 hexahedrons. Notably, a comparative gas-sensing study clearly revealed that the ZnO/α-Fe_2O_3 composites exhibited better acetone-sensing properties, including much higher and even faster response, when compared to the pure α-Fe_2O_3 hexahedrons. The remarkable improvement of sensing performances is most likely assigned to the striking synergistic effect and the small size of ZnO nanoparticles, which reaches a scale comparable to the ZnO Debye length.

■ ASSOCIATED CONTENT

Ⓢ Supporting Information

Plot displaying five periods of response−recovery curve. This material is available free of charge via the Internet at http://pubs.acs.org.

■ AUTHOR INFORMATION

Corresponding Authors

*Phone: +86 431 85167808. Fax: +86 431 85167808. E-mail: spmaster2008@163.com. (P.S.)

*E-mail: lugy@jlu.edu.cn. (G.L.)

Author Contributions

The manuscript was written through contributions of all authors. All authors have given approval to the final version of the manuscript.

Notes

The authors declare no competing financial interest.

■ ACKNOWLEDGMENTS

This work is supported by the National Nature Science Foundation of China (Nos. 61374218, 61134010, and 61327804) and Program for Chang Jiang Scholars and Innovative Research Team in University (No. IRT13018). National High-Tech Research and Development Program of China (863 Program, No. 2013AA030902 and 2014AA06A505).

■ ABBREVIATIONS

XRD, X-ray power diffraction
FESEM, field emission scanning electron microscopy
TEM, transmission electron microscopy
HRTEM, high-resolution transmission electron microscopy
EDS, energy-dispersive X-ray spectrometry
HMT, $(CH_2)_6N_4$
EG, ethylene glycol

■ REFERENCES

(1) Kim, H.-J.; Choi, K.-I.; Kim, K.-M.; Na, C. W.; Lee, J.-H. Highly Sensitive C_2H_5OH Sensors Using Fe-doped NiO Hollow Spheres. *Sens. Actuators, B* **2012**, *171−172*, 1029−1037.

(2) Alenezi, M. R.; Henley, S. J.; Emerson, N. G.; Silva, S. Ravi From 1D and 2D ZnO Nanostructures to 3D Hierarchical Structures with Enhanced Gas Sensing Properties. *Nanoscale* **2014**, *6*, 235−247.

(3) Rai, P.; Kwak, W.-K.; Yu, Y.-T. Solvothermal Synthesis of ZnO Nanostructures and Their Morphology-Dependent Gas-Sensing Properties. *ACS Appl. Mater. Interfaces* **2013**, *5*, 3026−3032.

(4) Sun, P.; Wang, W. N.; Liu, Y. P.; Sun, Y. F.; Ma, J.; Lu, G. Y. Hydrothermal Synthesis of 3D Urchin-like α-Fe_2O_3 Nanostructure for Gas Sensor. *Sens. Actuators, B* **2012**, *173*, 52−57.

(5) Agarwala, S.; Lim, Z. H.; Nicholson, E.; Ho, G. W. Probing the Morphology-Device Relation of Fe_2O_3 Nanostructures towards Photovoltaic and Sensing Applications. *Nanoscale* **2012**, *4*, 194−205.

(6) Li, X. L.; Lou, T. J.; Sun, X. M.; Li, Y. D. Highly Sensitive WO_3 Hollow-Sphere Gas Sensors. *Inorg. Chem.* **2004**, *43*, 5442−5449.

(7) Wang, L.; Teleki, A.; Pratsinis, S. E.; Gouma, P. I. Ferroelectric WO_3 Nanoparticles for Acetone Selective Detection. *Chem. Mater.* **2008**, *20*, 4794−4796.

(8) Waitz, T.; Wagner, T.; Sauewasld, T.; Kohl, C. D.; Tiemann, M. Ordered Mesoporous In_2O_3: Synthesis by Structure Replication and Application as a Methane Gas Sensor. *Adv. Funct. Mater.* **2009**, *19*, 653−661.

(9) Sun, X. H.; Hao, H. R.; Ji, H. M.; Li, X. L.; Cai, S.; Zheng, C. M. Nanocasting Synthesis of In_2O_3 with Appropriate Mesostructured Ordering and Enhanced Gas-Sensing Property. *ACS Appl. Mater. Interfaces* **2014**, *6*, 401−409.

(10) Chiu, H.; Yeh, C.-S. Hydrothermal Synthesis of SnO_2 Nanoparticles and Their Gas-Sensing of Alcohol. *J. Phys. Chem. C* **2007**, *111*, 7256−7259.

(11) Sun, P.; Zhao, W.; Cao, Y.; Guan, Y.; Sun, Y. F.; Lu, G. Y. Porous SnO_2 Hierarchical Nanosheets: Hydrothermal Preparation, Growth Mechanism, and Gas Sensing Properties. *CrystEngComm* **2011**, *13*, 3718−3724.

(12) Wang, C.; Cheng, X. Y.; Zhou, X.; Sun, P.; Hu, X. L.; Shimanoe, K.; Lu, G. Y.; Yamazoe, N. Hierarchical α-Fe_2O_3/NiO Composites with a Hollow Structure for a Gas Sensor. *ACS Appl. Mater. Interfaces* **2014**, *6*, 12031−12037.

(13) Ge, C. Q.; Xie, C. S.; Cai, S. Z. Preparation and Gas-sensing Properties of Ce-doped ZnO Thin-Film Sensors by Dip-Coating. *Mater. Sci. Eng., B* **2007**, *137*, 53−58.

(14) Wang, X. D.; Zhou, J.; Lao, C. S.; Song, J. H.; Xu, N. S.; Wang, Z. L. In Situ Field Emission of Density-Controlled ZnO Nanowire Arrays. *Adv. Mater.* **2007**, *19*, 1627−1631.

(15) Niu, X. S.; Du, W. P.; Du, W. M. Preparation and Gas Sensing Properties of ZnM_2O_4 (M=Fe, Co, Cr). *Sens. Actuators, B* **2004**, *99*, 405−409.

(16) Sun, P.; Cai, Y. X.; Du, S. S.; Xu, X. M.; You, L.; Ma, J.; Liu, F. M.; Liang, X. S.; Sun, Y. F.; Lu, G. Y. Hierarchical α-Fe_2O_3/SnO_2 Semiconductor Composites: Hydrothermal Synthesis and Gas Sensing Properties. *Sens. Actuators, B* **2013**, *182*, 336−343.

DOI: 10.1021/acsami.5b01071
ACS Appl. Mater. Interfaces 2015, 7, 8743−8749

(17) Chen, Y. J.; Zhu, C. L.; Wang, L. J.; Cao, P.; Cao, M. S.; Shi, X. L. Synthesis and Enhanced Ethanol Sensing Characteristics of α-Fe_2O_3/SnO_2 Core−Shell Nanorods. *Nanotechnology* **2009**, *20*, 045502.

(18) Huang, H.; Gong, H.; Chow, C. L.; Guo, J.; White, T. J.; Tse, M. S.; Tan, O. K. Low-Temperature Growth of SnO_2 Nanorod Arrays and Tunable n−p−n Sensing Response of a ZnO/SnO_2 Heterojunction for Exclusive Hydrogen Sensors. *Adv. Funct. Mater.* **2011**, *21*, 2680−2686.

(19) Li, C. C.; Yin, X. M.; Li, Q. H.; Wang, T. H. Enhanced Gas Sensing Properties of ZnO/SnO_2 Hierarchical Architectures by Glucose-Induced Attachment. *CrystEngComm* **2011**, *13*, 1557−1563.

(20) Zhang, D. F.; Sun, L. D.; Jia, C. J.; Yan, Z. G.; You, L. P.; Yan, C. H. Hierarchical Assembly of SnO_2 Nanorod Arrays on α-Fe_2O_3 Nanotubes: A Case of Interfacial Lattice Compatibility. *J. Am. Chem. Soc.* **2005**, *127*, 13492−1349.

(21) Xu, J.; Huang, F.; Yu, Y. L.; Yang, A. P.; Wang, Y. S. SnO_2/α-Fe_2O_3 Nanoheterostructure with Novel Architecture: Structural Characteristics and Photocatalytic Properties. *CrystEngComm* **2011**, *13*, 4873−4877.

(22) Kaneti, Y. V.; Zakaria, Q. M. D.; Zhang, Z. J.; Chen, C. Y.; Yue, J.; Liu, M. S.; Jiang, X. C.; Yu, A. B. Solvothermal Synthesis of ZnO-Decorated α-Fe_2O_3 Nanorods with Highly Enhanced Gas-Sensing Performance toward n-butanol. *J. Mater. Chem. A* **2014**, *2*, 13283−13292.

(23) Zhou, X.; Wang, C.; Feng, W.; Sun, P.; Li, X. W.; Lu, G. Y. Hollow α-Fe_2O_3 Quasi-Cubic Structures: Hydrothermal Synthesis and Gas Sensing Properties. *Mater. Lett.* **2014**, *120*, 5−8.

(24) Wang, D. W.; Du, S. S.; Zhou, X.; Wang, B.; Ma, J.; Sun, P.; Sun, Y. F.; Lu, G. Y. Template-Free Synthesis and Gas Sensing Properties of Hierarchical Hollow ZnO Microspheres. *CrystEngComm* **2013**, *15*, 7438−7442.

(25) Patil, D.; Patil, V.; Patil, P. Highly Sensitive and Selective LPG Sensor Based on α-Fe_2O_3 Nanorods. *Sens. Actuators, B* **2011**, *152*, 299−306.

(26) Rao, J.; Yu, A.; Shao, C. L.; Zhou, X. F. Construction of Hollow and Mesoporous ZnO Microsphere: A Facile Synthesis and Sensing Property. *ACS Appl. Mater. Interfaces* **2012**, *4*, 5346−5352.

(27) Zhang, L.; Du, L. H.; Yu, X.; Tan, S. Z.; Cai, X.; Yang, P. H.; Gu, Y.; Mai, W. J. Significantly Enhanced Photocatalytic Activities and Charge Separation Mechanism of Pd-Decorated ZnO−Graphene Oxide Nanocomposites. *ACS Appl. Mater. Interfaces* **2014**, *6*, 3623−3629.

(28) Wei, Y. H.; Han, S. B.; Walker, D. A.; Warren, S. C.; Grzybowski, B. A. Enhanced Photocatalytic Activity of Hybrid Fe_2O_3−Pd Nanoparticulate Catalysts. *Chem. Sci.* **2012**, *3*, 1090−1094.

(29) Garcia, M. A.; Merino, J. M.; Pinel, E. F.; Quesada, A.; Venta, J. D.; Gonzalez, M. L. R.; Castro, G. R.; Crespo, P.; Liopis, J.; Calbet, J. M. G.; Hernando, A. Magnetic Properties of ZnO Nanoparticles. *Nano Lett.* **2007**, *7*, 1489−1494.

(30) Ma, J. M.; Lian, J. B.; Duan, X. C.; Liu, X. D.; Zheng, W. J. α-Fe_2O_3: Hydrothermal Synthesis, Magnetic and Electrochemical Properties. *J. Phys. Chem. C* **2010**, *114*, 10671−10676.

(31) Kwon, K.-A.; Lim, H.-S.; Sun, Y.-K.; Suh, K.-D. α-Fe_2O_3 Submicron Spheres with Hollow and Macroporous Structures as High-Performance Anode Materials for Lithium Ion Batteries. *J. Phys. Chem. C* **2014**, *118*, 2897−2907.

(32) Park, K. T.; Xia, F.; Kim, S. W.; Kim, S. B.; Song, T.; Paik, U.; Park, W. I. Facile Synthesis of Ultrathin ZnO Nanotubes with Well-Organized Hexagonal Nanowalls and Sealed Layouts: Applications for Lithium Ion Battery Anodes. *J. Phys. Chem. C* **2013**, *117*, 1037−1043.

(33) Huang, J.; Yin, Z. G.; Zheng, Q. D. Applications of ZnO in Organic and Hybrid Solar Cells. *Energy Environ. Sci.* **2011**, *4*, 3861−3877.

(34) Niu, H. H.; Zhang, S. W.; Ma, Q.; Qin, S. X.; Wan, L.; Xu, J. Z.; Miao, S. D. Dye-Sensitized Solar Sells Based on Flower-Shaped α-Fe_2O_3 as a Photoanode and Reduced Graphene Oxide−Polyaniline Composite as a Counter Electrode. *RSC Adv.* **2013**, *3*, 17228−17235.

(35) Wu, W.; Zhang, S. F.; Xiao, X. H.; Zhou, J.; Ren, F.; Sun, L. L.; Jiang, C. Z. Controllable Synthesis, Magnetic Properties, and Enhanced Photocatalytic Activity of Spindlelike Mesoporous α-Fe_2O_3/ZnO Core−Shell Heterostructures. *ACS Appl. Mater. Interfaces* **2012**, *4*, 3602−3609.

(36) Zhang, J.; Liu, X. H.; Wang, L. W.; Yang, T. L.; Guo, X. Z.; Wu, S. H.; Wang, S. R.; Zhang, S. M. Synthesis and Gas Sensing Properties of α-Fe_2O_3@ZnO Core−Shell Nanospindles. *Nanotechnology* **2011**, *22*, 185501.

(37) Sun, P.; Liu, Y. W.; Li, X. W.; Sun, Y. F.; Liang, X. S.; Liu, F. M.; Lu, G. Y. Facile Synthesis and Gas-sensing Properties of Monodisperse α-Fe_2O_3 Discoid Crystals. *RSC Adv.* **2012**, *2*, 9824−9829.

(38) Sun, P.; You, L.; Wang, D. W.; Sun, Y. F.; Ma, J.; Lu, G. Y. Synthesis and Gas Sensing Properties of Bundle-like α-Fe_2O_3 Nanorods. *Sens. Actuators, B* **2011**, *156*, 368−374.

(39) Lou, Z.; Li, F.; Deng, J. N.; Wang, L. L.; Zhang, T. Branch-like Hierarchical Heterostructure (α-Fe_2O_3/TiO_2): A Novel Sensing Material for Trimethylamine Gas Sensor. *ACS Appl. Mater. Interfaces* **2013**, *5*, 12310−12316.

(40) Wang, S. M.; Xiao, B. X.; Yang, T. Y.; Wang, P.; Xiao, C. H.; Li, Z. F.; Zhao, R.; Zhang, M. Z. Enhanced HCHO Gas Sensing Properties by Ag-Loaded Sunflower-like In_2O_3 Hierarchical Nanostructures. *J. Mater. Chem. A* **2014**, *2*, 6598−6604.

(41) Sun, P.; Sun, Y. F.; Ma, J.; You, L.; Lu, G. Y.; Fu, W. Y.; Li, M. H.; Yang, H. B. Synthesis of Novel $SnO_2/ZnSnO_3$ Core−Shell Microspheres and Their Gas Sensing Properities. *Sens. Actuators, B* **2011**, *155*, 606−611.

(42) Neri, G.; Bonavita, A.; Micali, G.; Rizzo, G.; Callone, E.; Carturan, G. Resistive CO Gas Sensors Based on In_2O_3 and $InSnO_x$ Nanopowders Synthesized via Starch-aided Sol−Gel Process for Automotive Applications. *Sens. Actuators, B* **2008**, *132*, 224−233.

(43) Dayan, N. J.; Sainkar, S. R.; Karekar, R. N.; Aiyer, R. C. Formulation and Characterization of ZnO: Sb Thick-Film Gas Sensors. *Thin Solid Films* **1998**, *325*, 254−258.

(44) Zeng, S. Y.; Tang, K. B.; Li, T. W.; Liang, Z. H.; Wang, D.; Wang, Y. K.; Qi, Y. X.; Zhou, W. W. Facile Route for the Fabrication of Porous Hematite Nanoflowers: Its Synthesis, Growth Mechanism, Application in the Lithium Ion Battery, and Magnetic and Photocatalytic Properties. *J. Phys. Chem. C* **2008**, *112*, 4836−4843.

(45) Lian, S. Y.; Li, H. T.; He, X. D.; Kang, Z. H.; Liu, Y.; Lee, S. T. Hematite Homogeneous Core/Shell Hierarchical Spheres: Surfactant-Free Solvothermal Preparation and Their Improved Catalytic Property of Selective Oxidation. *J. Solid State Chem.* **2012**, *185*, 117−123.

(46) Liu, X. J.; Chang, Z.; Luo, L.; Lei, X. D.; Liu, J. F.; Sun, X. M. Sea Urchin-like Ag−α-Fe_2O_3 Nanocomposite Microspheres: Synthesis and Gas Sensing Applications. *J. Mater. Chem.* **2012**, *22*, 7232−7238.

(47) Yamazoe, N. New Approaches for Improving Semiconductor Gas Sensors. *Sens. Actuators, B* **1991**, *5*, 7−19.

(48) Egashira, M.; Shimizu, Y.; Takao, Y.; Sako, S. Variations in I-V Characteristics of Oxide Semiconductors Induced by Oxidizing Gases. *Sens. Actuators, B* **1996**, *35*−*36*, 62−67.

(49) Chi, X.; Liu, C. B.; Liu, L.; Li, Y.; Wang, Z. J.; Bo, X. Q.; Liu, L. L.; Su, C. Tungsten Trioxide Nanotubes with High Sensitive and Selective Properties to Acetone. *Sens. Actuators, B* **2014**, *194*, 33−37.

(50) Gao, T.; Wang, T. H. Synthesis and Properties of Multipod-Shaped ZnO Nanorods for Gas-Sensor Applications. *Appl. Phys. A: Mater. Sci. Process.* **2005**, *80*, 1451−1454.

(51) Vuong, N. M.; Hieu, N. M.; Hieu, H. N.; Yi, H.; Kim, D.; Han, Y.-S.; Kim, M. Ni_2O_3-Decorated SnO_2 Particulate Films for Methane Gas Sensors. *Sens. Actuators, B* **2014**, *192*, 327−333.

(52) Lee, J.-H. Gas Sensors Using Hierarchical and Hollow Oxide Nanostructures: Overview. *Sens. Actuators, B* **2009**, *140*, 319−336.

(53) Yamazoe, N.; Sakai, G.; Shimanoe, K. Oxide Semiconductor Gas Sensors. *Catal. Surv. Asia* **2003**, *7*, 63−75.

(54) Yao, M. S.; Hu, P.; Han, N.; Ding, F.; Yin, C. L.; Yuan, F. L.; Yang, J.; Chen, Y. F. ZnO Micro-Windbreak for Enhanced Gas Diffusion. *Sens. Actuators, B* **2013**, *186*, 614−621.

DOI: 10.1021/acsami.5b01071
ACS Appl. Mater. Interfaces 2015, 7, 8743−8749